Int. Conf. on Computational Methods for Coupled Problems in Science and Engineering
COUPLED PROBLEMS 2005
M. Papadrakakis, E. Oñate and B. Schrefler (Eds)
©CIMNE, Barcelona, 2005

COUPLING FINITE AND SEMI-INFINITE DOMAINS WITH APPLICATIONS TO SOIL STRUCTURE INTERACTION

E. A. Malsch* **and L. Lehmann†**

*Institut für Angewandte Mechanik
Technische Universität Braunscheweig
Spielmannstraße 11,D-38160 Braunschweig, Germany
e-mail: malsch@civil.columbia.edu

e-mail: lutz-o.lehmann@tu-bs.de

Key words: Coupled Problems, Soil-structure interaction, Cloning algorithm

Abstract. *Numerical modeling of soil-structure interaction requires efficient methods for modeling unbounded domains. Discretizing large-domains into many small finite elements is often inconvenient, inefficient or impossible. The Boundary Element method, while well suited to unbounded geometries, can not be applied to all materials. The cloning-algorithm is an alternative method which can be applied independently of the field equation, and reproduces the both the near and the far-field boundary conditions. Using the method, infinite and semi-infinite domains can be modeled using finite elements provided the materials properties such as stiffness, mass and damping have proportional values in proportional geometries. The cloning algorithm allows for the construction of shape functions which satisfy the essential boundary conditions, including the far-field radiation condition. The shape functions do not necessarily satisfy any given field equation. In this presentation, to ensure an efficient modeling of the intermediate domain, between the very near and very far fields, the cloning is performed cells that are not infinitely thin. Instead, shape functions which model concave domains are employed. The results are compared to the standard infinite cell approach.*

1 INTRODUCTION

The *infinite element* or *cloning* method was first developed independently by Ying in 1978, in Chinese, and Dasgupta in 1982 [22, 7]. It relies on the calculation of the mechanical properties of a finite cell whose geometry is determined by the shape of the near-field boundary. Wolf and Song have been developing extensions and refinements to the the cloning algorithm for the past twenty years [21], further developments have been made others including Deeks [8], Crouch and Bennett [5] and Lehmann et. al [12]. In particular, the Scaled Boundary Finite Element method is a version of the cloning

algorithm which uses a infinitely thin cell. Since only the near field boundary needs to be discretized the approach reduces the dimension of the cell domain. Unfortunately, while the infinitely thin cell can be used to capture the effect of the infinite domain, it can not be used to describe its behavior. The cells with a finite width, used in this presentation, prescribe the behavior at every point in the domain.

In general, if the behavior of the domain with respect to a given input and response can be modeled by using an elliptic differential operator then approximate solutions are formulated to satisfy either the essential boundary conditions or the operator within the domain. The exact solution satisfies both boundary conditions and the field equation. The approximate method which satisfies the boundary conditions is the Rayleigh-Ritz method, and the Boundary Element and other Green's function related methods satisfy the field equation [18]. Field dependent methods are well suited to unbounded domains because they satisfy the far-field decay, or Sommerfeld-Radiation, conditions [6, 3].

Approximations which satisfy only the near-field boundary conditions can simulate an infinite domain by imposing special kinds of boundary conditions relatively far away from the near-field [1]. Similarly, approaches which satisfy only the far-field boundary behavior but not the near-field essential boundary conditions produce reasonable results only in the far field [9, 4]. Approximate solutions which satisfy the essential boundary conditions in the near field and simulate the decay can similarly produce reasonable approximations in specific applications [2, 17]. None of the available field independent methods, except cloning type algorithms, satisfy both the radiation-damping condition and the essential geometric boundary conditions in the near and far fields [20].

2 PROPORTIONAL PARTITIONING

In the presented modified finite element formulation, computation and integration only needs to be preformed near the small scale inclusions. The regularity of the large scale domain is exploited to reduce the area where integration is required. Elements or cells, with similar geometry have similar mechanical properties. On homogeneous domains, for example, the stiffness and mass matrices are proportional. Accordingly, the mechanical properties of only one representative element need to be calculated. It is convenient to choose the smallest cell, the one closest to the small scale inclusion or indentation, see Figs. 1 and 2.

The cloning algorithm applies only when the material properties within two geometrically similar domains are similar with respect to the scale of the domains. In homogeneous domains, for example, the stiffness and mass matrices are proportional:

$$[K_A] = \left(\frac{l_a}{l_b}\right)^{(\kappa-2)} [K_B] \quad \text{and} \quad [M_A] = \left(\frac{l_a}{l_b}\right)^{(\kappa-1)} [M_B] \tag{1}$$

Where κ is 2 or 3 depending whether the model is in two or three dimensions respectively. Also, l_i is the characteristic length measure of the i^{th} element. Provided the proportional-

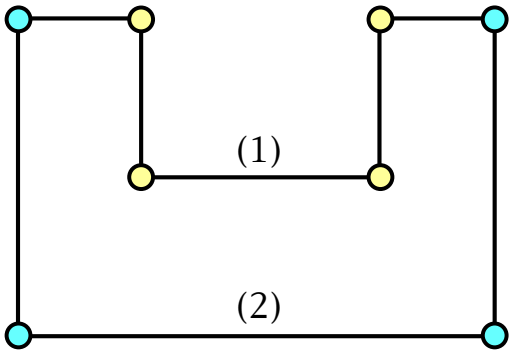


Figure 1: Single cell.

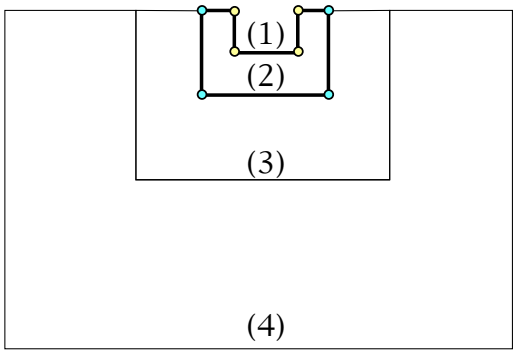


Figure 2: Proportionally sized cells.

ity requirement also applies when the material behavior is nonlinear or anisotropic, such a material can also be represented within the constructs of the cloning algorithm.

In any domain where the stiffness of two geometrically similar cells is also similar the following simplification can be applied on cells which are seated within one another, see Fig. 2:

$$\left[\begin{array}{c|c} K_{11} & K_{12} \\ \hline K_{21} & K_{22} \end{array}\right] \left\{ \begin{array}{c} \{u_1\} \\ \{u_2\} \end{array} \right\} = \left\{ \begin{array}{c} \{f_1\} \\ \{f_2\} \end{array} \right\} \quad \text{and} \quad \left[\begin{array}{c|c} \hat{K}_{22} & \hat{K}_{23} \\ \hline \hat{K}_{32} & \hat{K}_{33} \end{array}\right] \left\{ \begin{array}{c} \{u_2\} \\ \{u_3\} \end{array} \right\} = \left\{ \begin{array}{c} -\{f_2\} \\ \{f_3\} \end{array} \right\}. \quad (2)$$

And the stiffness matrix is similarly proportional between adjacent cells:

$$\alpha \left[\begin{array}{c|c} K_{11} & K_{12} \\ \hline K_{21} & K_{22} \end{array}\right] = \left[\begin{array}{c|c} \hat{K}_{22} & \hat{K}_{23} \\ \hline \hat{K}_{32} & \hat{K}_{33} \end{array}\right] \quad (3)$$

Separating Eq. 2, and using the equilibrium at the shared cell boundary leads to the following:

$$\begin{aligned} [K_{11}]\{u_1\} + [K_{12}]\{u_2\} &= \{f_1\} && (4) \\ [K_{21}]\{u_1\} + ([K_{22}] + \alpha[K_{11}])\{u_2\} + \alpha[K_{12}]\{u_3\} &= \{0\} && (5) \\ \alpha[K_{21}]\{u_2\} + \alpha[K_{22}]\{u_3\} &= \{f_3\} && (6) \end{aligned}$$

2.1 Finite domains

A set n geometrically similar cells define the behavior of a domain. Given a small inclusion or indentation of characteristic length r_0 and a scaling factor ξ, the size of the domain described by the n cells is:

$$r_n = \alpha^n r_0 \quad (7)$$

Then the banded stiffness matrix of the domain is defined completely by the stiffness of on of the cells:

$$\begin{bmatrix} K_{11} & K_{12} & \dots & 0 & 0 \\ K_{21} & K_{22}+\alpha K_{11} & \dots & 0 & 0 \\ \vdots & \vdots & \ddots & \vdots & \vdots \\ 0 & 0 & \dots & \alpha^{n-1}K_{22}+\alpha^n K_{11} & \alpha^n K_{12} \\ 0 & 0 & \dots & \alpha^n K_{21} & \alpha^n K_{22} \end{bmatrix} \begin{Bmatrix} \{u_1\} \\ \{u_2\} \\ \vdots \\ \{u_{n-1}\} \\ \{u_n\} \end{Bmatrix} = \begin{Bmatrix} \{f_1\} \\ \{0\} \\ \vdots \\ \{0\} \\ \{f_n\} \end{Bmatrix} \tag{8}$$

The dimension of the matrix could be reduced using static condensation. In general, the internal forces are not zero in either Eq. 8 or Eq. 6 if body forces are acting upon the element.

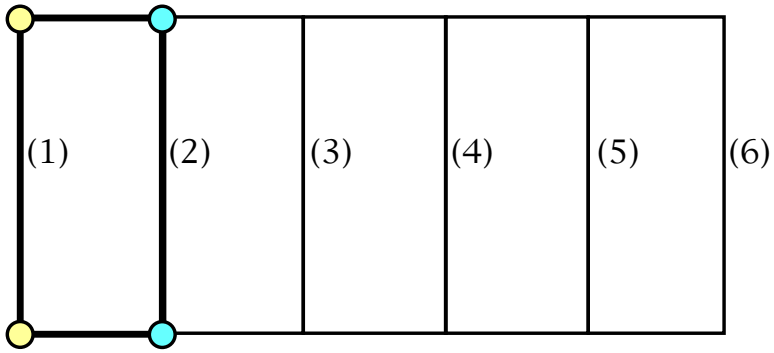


Figure 3: Simple mesh generated from a single cell.

For example, on the simple mesh in Fig. 3 the stiffness of the cell with boundaries (1) and (2) defines the stiffness of the domain from boundary (1) to boundary (6). The eigenvalues of the representative cell, with material properties $E = 100MN/m^2$ and $\nu = \frac{1}{3}$:

$$(322.7, 103.1, 52.29, 46.88, 37.50, 0, 0, 0) \tag{9}$$

The range of the eigenvalues of the expanded domain are:

$$(572.4, \dots, 4.527, 0, 0, 0) \tag{10}$$

As expected, the combination of cells does not add any spurious modes. Also, the eigenvalues are of the same order of magnitude. This reflects the numerical stability of the conventional finite element approach well explored in other references [23]. Adding a node at the mid point of each edge the eigenvalues for the representative cell:

$$(423.3, 334.5, 178.6, 142.6, 111.9, 103.9, 59.35, 49.70, 48.35, 0, 0, 0)\,, \tag{11}$$

the range of eigenvalues of the expanded domain is:

$$(827.8, \dots, 3.972, 0, 0, 0, 0)\,. \tag{12}$$

In its application the approach is the standard finite element method with expected $O(h^2)$ convergence rate [19].

Similarly, the stiffness of the single cell in Fig. 1 describes the properties of the set of cells Fig. 2 . The square indentation has a width w and a height h. The indentation is located on a proportional domain with width W and height H where:

$$W = \alpha^n w \quad \text{and} \quad H = \alpha^n h \tag{13}$$

where α is the scaling factor, see Eq. 3, and n is the number of cells in the domain. Since n is an integer it is convenient to derive the scaling factor from the dimensions of the domain and the desired number of cells:

$$\alpha = \left(\frac{W}{w}\right)^{\frac{1}{n}} = \left(\frac{H}{h}\right)^{\frac{1}{n}} \tag{14}$$

The expected convergence rate for a standard finite element mesh mindful that the characteristic length h increases exponentially with distance.

2.2 Infinite and semi-infinite domains

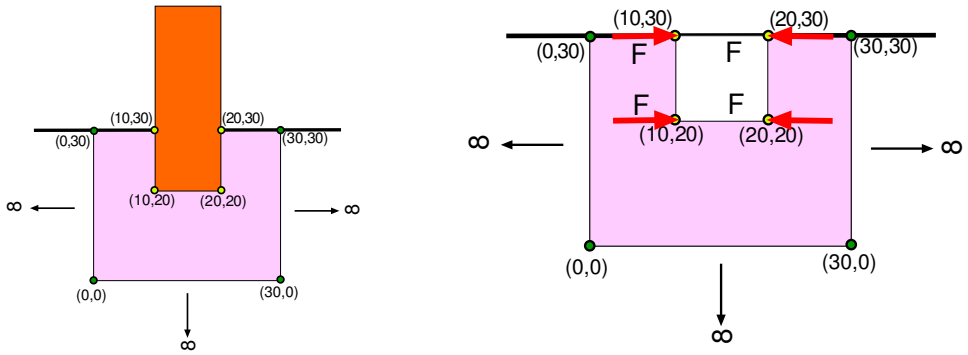


Figure 4: Two dimensional footing. Lengths in [m].

The near-field boundary is located at the interface between the soil and the structure, see Fig. 4. The shape of the boundary is determined by the shape of the foundation. Only a cell with two boundaries similar to the foundation shapes needs to be modeled in the analysis, see Fig. 2. The forces and displacements on the near-field boundary (1) and the geometrically similar boundary (2) are related by compatibility and equilibrium to the forces and displacements of two separate semi-infinite domains. Boundary (1) is the surface of the first domain (A) and boundary (2) the surface of the second domain (B).

The following function describes the relationship between either static or dynamic stiffness in the two geometrically similar semi-infinite domains (A) and (B). Equilibrium and compatibility at the surfaces leads to the following static stiffness equation:

$$[K_A^*] = [K_{11}] - [K_{12}]([K_B^*] + [K_{22}])^{-1}[K_{21}]. \tag{15}$$

The details of the derivation are given in the reference [7]. The same results can be found by applying static condensation and letting the combined matrix in Eq. 8 approach infinity [22]. If the stiffnesses of the two geometrically similar unbounded media are proportional then define:

$$[K^*] = [K^*_A] = \frac{1}{\xi}[K^*_B]. \tag{16}$$

The quadratic matrix equation can be solved using a number of methods [10]. For example, define the following:

$$\begin{aligned} [Y] &= (\xi[K] + [K_{22}])[K_{21}]^{-1}, \\ [Q] &= (\xi[K_{11}] + [K_{22}])[K_{21}]^{-1}, \\ [R] &= \xi[K_{12}][K_{21}]^{-1}. \end{aligned} \tag{17}$$

Using the definitions from Eq. 17, the surface equilibrium equation, Eq. 15, can be rewritten as a standard quadratic matrix equation:

$$[Y][Y] - [Q][Y] + [R] = 0. \tag{18}$$

To rewrite the quadratic matrix equation as a quadratic eigenvalue problem post-multiply by an eigenvector $\{y_i\}$ where $[Y]\{y_i\} = \xi_i\{y_i\}$:

$$(\xi_i^2 - [Q]\xi_i + [R])\{y_i\} = 0. \tag{19}$$

Using the cloning algorithm, the stiffness of a concave cell defines the stiffness of the unbounded media.

When $[K_{11}]$ and $[K_{22}]$ are symmetric all eigenvalues not associated with rigid body modes of the unbounded domain are strictly greater than zero. For the derivation see the reference [7]. In a two dimensional domain the rigid body translation modes are not damped and consequently the stiffness of the unbounded domain has two zero eigenvalues. Consequently, for every case, except the two-dimensional domain, the cloning-algorithm returns a stiffness matrix for the unbounded medium which is positive definite. This result is also evident in exact analytical solutions [11]

2.2.1 Anisotropic proportionality

The stiffness of the unbounded domain is a nonlinear function of the stiffness of the representative cell, see Eq. 18. Consequently, a linear combination of stiffnesses is not linear combination of their corresponding stiffness in unbounded domains. For example, the stiffness of each of the cells in the mesh shown in Fig. 5 have proportional $[K^{xx}]$ and $[K^{yy}]$ components, see Appendix A.1. Scaling only the width of the cell has the following effect on the stiffness matrix:

$$[K^*_a] = [P^*] + [Q^*] + [R^*] \quad \text{and} \quad [K^*_b] = \frac{1}{\xi}[P^*] + [Q^*] + \xi[R^*]. \tag{20}$$

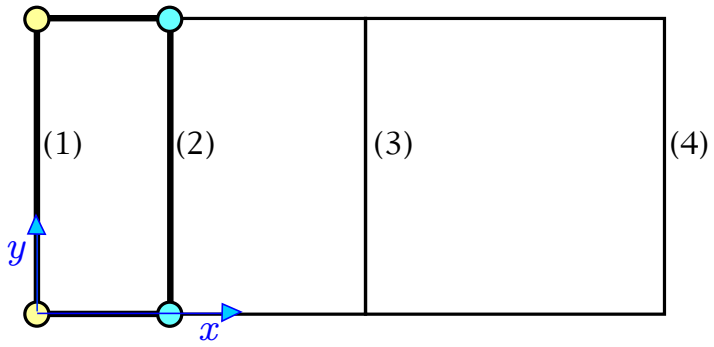


Figure 5: Simple mesh with an anisotropic deformation.

The associated quadratic matrix equation is:

$$[K^{ab}]^{-1}\left([K_a^*]-([P^*]+[Q^*]+[R^*])\right)=\left([K_b^*]+\left(\frac{1}{\xi}[P^*]+[Q^*]+\xi[R^*]\right)\right)^{-1}[K^{ba}]. \quad (21)$$

The solution to this anisotropic problem can not be solved simply simply considering each matrix independently. Instead a series solution can be employed. Methods for solving such problems are covered extensively in the references [22] and [21]. The nonlinearity arises in the static condensation. Consequently, for finite domains a stiffness matrix, such as in Eq. 8, can be constructed. Furthermore, in the far field when n is large and ξ^n is large enough, the $[R^*]$ matrix controls the solution behavior and can be solved for using the standard method for one matrix, see Eq. 18.

3 MODELING THE REPRESENTATIVE CELL

The representative cell is the only element upon which the stiffness needs to be evaluated. Due to the symmetry in the method, errors in the representation of the stiffness of the representative cell can lead to an overly stiff representation of the larger domain. To avoid any locking of this type, it is beneficial to model the cell with a more accurate approach even if it is relatively slow. This dependence on the cell model may be a reason thick cells are not commonly employed in dynamic applications of the cloning method. The cloning algorithm is most stable when the stiffness of the concave slice is represented by a fully populated matrix. Nevertheless, sparse matrices can be employed provided some of the interaction between the two boundaries is captured provided $\det[K_{21}] \neq 0$ and $\det[K_{12}] \neq 0$ in Eq. 15.

3.1 Mesh of triangles

It is possible to model the representative element using a standard triangular mesh on the representative cell. Follow the standard shape functions and integration procedures [23]. For example model the cell in Fig. 1 using the mesh in Fig. 6. For this model problem let $E = 100MN/m^2$ and $\nu = 0.3$, the eigenvalues and displacement results are summarized

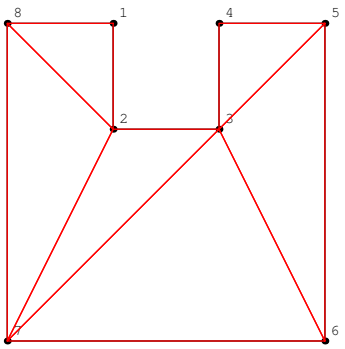


Figure 6: Simple triangular mesh

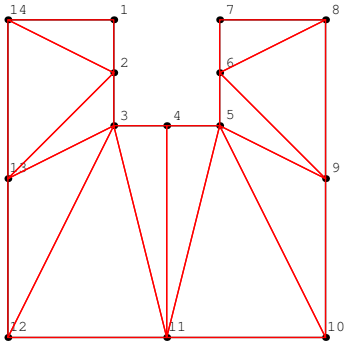


Figure 7: One side node.

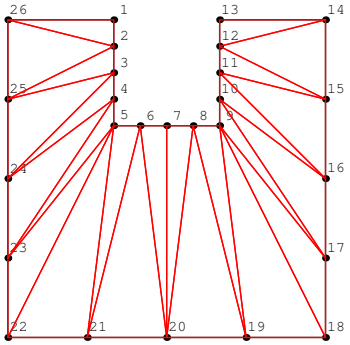


Figure 8: Two side nodes.

in Table 1. The horizontal displacement at the surface incurred at the boundary of the

Table 1: Comparing meshed models of the representative cell and unbounded domain.

		REP. CELL		UNBOUNDED CELL		
ξ	side nodes	min. eig.	max. eig.	min. eig.	max. eig.	max disp $[m]$.
3	0	13.74	704.3	36.40	539.0	0.1284
3	1	6.591	1001	27.57	877.8	0.1302
3	3	6.055	2439	18.53	2267	0.1038
1.5	0	4.301	856.4	39.02	357.0	0.09602
1.5	1	0.5696	648.3	16.30	291.0	0.1819
1.5	3	0.3308	744.3	8.290	506.3	0.2232
1.1	0	0.920	3175	45.01	388.4	0.0813
1.1	1	0.1530	2622	18.97	349.6	0.1465
1.1	3	0.02484	1379	7.827	292.5	0.2200

unbounded domain due to the loading in Fig. 4 is about: $0.13m$. The cell outer boundary of the cell in Fig. 1 is three times as large as the inner boundary, see Fig. 6. Performing the same cloning algorithm and displacement calculation on successively thinner cells with scaling factors $\xi = 1.5$ and 1.1, the surface displacements are $0.10m$ and $0.08m$ respectively. The result is counter intuitive, the smaller the cell gets the more flexible the result should be. If instead of making the cell thinner more nodes are added to the sides of the domain, such as in Figs. 7 and 8, the displacement at the surface computes to $0.13m$, $0.18m$ and $0.15m$ for one additional node on every side and scaling factors $\xi = 3$, 1.5 and 1.1 respectively. Again the displacement decreases as the cell is made smaller. Adding more nodes on the edges increases the accuracy of the approach but does not assure that a thinner cell returns a more accurate result.

Table 2: Test case results for a representative cell that is concave.

			REP. CELL		UNBOUNDED CELL		
ξ	step	h	min. eig.	max. eig.	min. eig.	max. eig.	max. disp.
3	0.2	0.02	17.17	453.4	36.84	347.3	0.1282
3	0.1	0.01	16.82	447.6	35.98	341.3	0.1313
1.5	0.1	0.04	3.537	840.3	29.67	284.6	0.1386
1.5	0.05	0.02	3.438	831.9	29.16	277.6	0.1424
1.1	0.02	0.04	0.5350	3803	28.81	328.4	0.1400
1.1	0.01	0.02	0.5244	3789	28.53	324.7	0.1416

3.2 Conformal shape function without a mesh

In the same model problem solved using the triangular mesh, conformal shape functions which do not require discretization are applied, see appendix A.2. Unlike the triangular case, numerical integration introduces error into the analysis. The results are collected in the Table 2. In this first example, the integration is handled as simply as possible. Find the derivatives of the shape functions in closed form by hand or using a computer algebra program, in this case *Mathematica*. Since the functions are smooth within the domain, a simple numerical algorithm is sufficient for the integration. Replace the integral with a sum with a step size h in both the x and y directions:

$$\iint_{\mathcal{D}} N_{i,x}(x,y) N_{j,x}(x,y) \mathrm{d}x\mathrm{d}y \approx h^2 \sum_{\forall (x_k,y_k)\in\mathcal{D}} \sum N_{i,x}(x_k,y_k) N_{j,x}(x_k,y_k). \tag{22}$$

The integration smoothes out the singular behavior of the differentiated function along the boundary segments. Since only one element is used to represent the entire foundation, the number of integration points depends on the smoothness of the shape function, not directly on the number of nodes. The order of approximation of the numerical algorithm is $O(h)$. The errors in the numerical tests are consistent with the estimate, see Table 2.

For an element described by only eight vertex nodes, see Fig. 4, the results are generally more accurate than for the triangular mesh with the same number of nodes, even if rather large errors are incurred in the numerical integration. The maximum displacement predicted by the triangular mesh is $0.13m$ and for the concave cell is $0.14m$. Unlike the triangular mesh case, using the smooth conformal shape functions, the more nodes an element had the more flexible it is.

It is not always convenient to find the analytical derivative of the shape function $N_i(x,y)$. The shape functions for elements with side nodes, for example, are quite complicated [13]. Evaluating the analytic derivative is significantly more time consuming than evaluating the numerical derivative. In such a case define the integral in Eq. 22 as follows:

$$h^2 \sum_{\forall (x_k,y_k)\in\mathcal{D}} \sum \left(\frac{N_i(x_k+\mathbf{h},y_k)-N_i(x_k,y_k)}{\mathbf{h}}\right)\left(\frac{N_j(x_k+\mathbf{h},y_k)-N_j(x_k,y_k)}{\mathbf{h}}\right) \tag{23}$$

The discretization of the differentiation **h** need not be equal to the discretization used in the integration h.

3.2.1 Additional nodes on the boundary

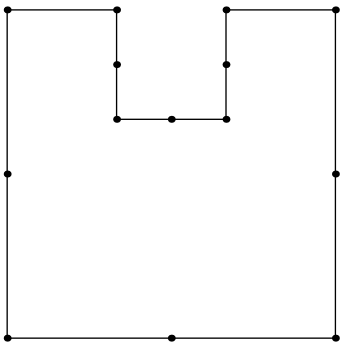


Figure 9: Concave cell with one side node.

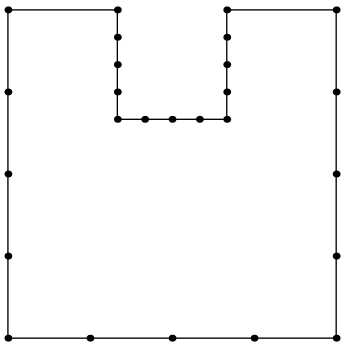


Figure 10: Concave cell with three side nodes.

Side nodes can be added to the representative cell without breaking the conformal nature of the interpolation using the method summarized in the reference [13]. The results for the test case are collected in Table 3. The displacement at the surface obtained using the Scaled Boundary Finite Element method with the same node configuration on the interior boundary as in Fig. 10 is $0.26m$. Neglecting the errors introduced by the numerical integration, the results should be more accurate than those for a triangular mesh with the same number of nodes. The goal is not achieved in this example. The integration error and numerical error in the calculation are especially detrimental since the smallest non-zero eigenvalues of the representative matrices are becoming quite small. Nevertheless, the displacement results correct are within the order of accuracy of the numerical calculation.

Table 3: Test case results for a representative cell with added nodes on the sides.

			REP. CELL		UNBOUNDED CELL		
ξ	step	h	min. eig.	max. eig.	min. eig.	max. eig.	max. disp.
One side node.							
3	0.1	0.01	13.13	2.772×10^5	24.72	2.738×10^3	0.1192
1.5	0.1	0.04	2.781	9.011×10^5	21.63	5.059×10^5	0.1287
1.5	0.05	0.02	2.703	2.741×10^5	21.07	1.521×10^5	0.1424
1.1	0.05	0.10	1.244×10^{-5}	3.682×10^4	2.433	2.694×10^4	0.1609
1.1	0.02	0.04	1.198×10^{-5}	2.453×10^4	2.442	4.181×10^4	0.1677
Three side nodes.							
1.1	0.05	0.10	6.440×10^{-6}	5.446×10^7	1.560	4.827×10^7	0.1609

4 COUPLED DOMAINS

The boundary nearest to the inclusion is modeled with finite elements and conformal shape functions. Coupling two meshes with nodes at the same locations and conformal edge behavior is trivial [23]. Similarly, finite domains modeled using a representative cell are coupled to one another using standard finite element approaches for C^0 interfaces. To this end, choose the location of the nodes on the boundary of the representative cell so that the far away boundary of the larger region matches node for node with its neighbors. Examples of such coupled domains include a half space without an indentation and a half space with an inclusion, see Figs. 11 and 12. For the purposes of coupling, only the behavior of the near boundary and the far away boundary are of interest, in Fig. 3, boundary (1) and (6). The entire matrix in Eq. 8 need not be solved, instead a transfer matrix which relates the displacement at one boundary. The transfer matrix is described in detail in the reference [22]. On the other hand, any coupling of the outside boundary which lies at infinity must already be evident within the representative cell.

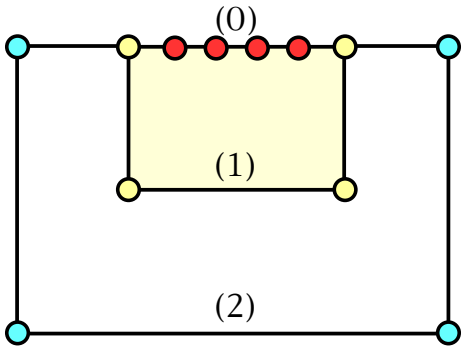


Figure 11: Coupling a finite and semi-infinite cell.

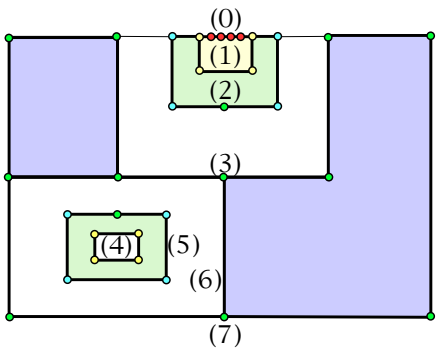


Figure 12: In-homogenous half space with an inclusion.

5 CONCLUSIONS

By exploiting the similarity of properties in geometrically similar domains the effect of a small scale behavior on a large scale domain can be modeled without integrating over the entire domain. Using representative elements with finite widths, the behavior of the near-field, far-field and intermediate domain is modeled explicitly. The method is extremely sensitive to the stiffness matrix of the representative element. Modeling the element using the standard triangular mesh tends to lead to overly stiff estimations. Shape functions which are conformal and smooth over the element domain seem to perform better. Provided the integration error is small enough, the shape functions which are conformal on polygons produce a result which is more accurate than the triangular mesh and less accurate than the Scaled Boundary Finite Element result.

The thick-cell cloning is especially efficient for modeling the behavior of the intermediate domain, where the Scaled Boundary Finite Element method does not apply. The

thick-cell cloning method satisfies the essential boundary conditions. As such, all of the interfaces to finite element meshes are conformal. In the examples presented in this paper, the entire semi-infinite domain the shape functions satisfy C^0 continuity and linear completeness. The error in the model is consistent with that derived for the standard finite element method on a finite domain. The behavior of the intermediate domain is governed by the coupling of the near and far field behaviors. The thick-celled cloning elements efficiently connect the very near near field to the very far fields while satisfying the Sommerfeld-radiation condition.

ACKNOWLEDGEMENT

The first author is grateful for the Alexander von Humboldt Fellowship that is supporting her participation in the CINME conference and her on-going research.

REFERENCES

[1] R. J. Astley. Infinite elements for wave problems: a review of current formulations and an assessment of accuracy. *International Journal for Numerical Methods in Engineering*, 49:pp. 951–976, 1999.

[2] Peter Bettess and O. C. Zienkiewicz. Diffraction and refraction of surface waves using finite and infinite elements. *International Journal for Numerical Methods in Engineering*, 11:pp,1271–1290, 1977.

[3] C. A. Brebbia and J. Dominguez. *Boundary Elements - An Introductory Course*. McGraw-Hill, 1992.

[4] Davis S. Burnett. A three-dimensional acoustic infinite element based on a prolate spheroidal multipole expansion. *The Journal of the Acoustical Society of America*, 96(5):pp. 2798–2816, November 1994.

[5] R. S. Crouch and T. Bennet. Efficient ebe treatment of the dynamic far-field in non-linear fe soil-structure interaction analyses. In *European Congress on Computational Methods in Applied Sciences and Engineering 2000*, Barcelona, 2000. ECCOMAS.

[6] S. L. Crouch and A. M. Starfield. *Boundary Element Methods in Solid Mechanics*. George Allen & Unwin, London, 1983.

[7] Gautam Dasgupta. A finite element formulation for unbounded homogeneous continua. *Journal of Applied Mechanics*, 104:136 — 140, 3 1982.

[8] A. Deeks and J.P. Wolf. An h-hierarchical adaptive procedure for the scaled boundary finite-element method. *International Journal for Numerical Methods in Engineering*, 54:585–605, 2002.

[9] S. Gupta, T.W. Lin, and J. Penzien. Hybrid modelling of soil-structure interaction. Technical Report 80/09, UCB/EERC, 1980.

[10] N. J. Higham and Hyun min Kim. Numerical analysis of a quadratic matrix equation. *IMA Journal of Numerical Analysis*, 20:499–519, 2000.

[11] K. L. Johnson. *Contact Mechanics*. Cambridge University Press, 1985.

[12] L. Lehmann, H. Antes, and M. Schanz. Transient analysis of soil-structure interaction problems: An effective fem/sbfem approach. In G. Rechard G.A. Holzapfel, W.Moser, editor, *Advanced Numerical Analyses of Solids and Structures, and Beyond*, pages 99–116, Graz, Austria, 2004. Institute for Structural Analysis, Verlag der Technischen Universität Graz.

[13] Elisabeth Malsch and Gautam Dasgupta. Interpolation constraints and thermal distributions: a method for all non-concave polygons. *International Journal of Solids and Structures*, 41(8):2165–2188, 2004.

[14] Elisabeth Malsch and Gautam Dasgupta. Smooth two dimensional interpolants: a recipe for all polygons. *Graphics Tools*, page (in press), 2004.

[15] Elisabeth A. Malsch and Gautam Dasgupta. Algebraic construction of smooth interpolants on polygonal domains. *Mathematica Journal*, page (in press), 2004.

[16] Elisabeth Anna Malsch. *Test functions for elliptic operators satisfying essential edge conditions on both convex and concave polygonal domains*. PhD thesis, Columbia University, 2003.

[17] F. Medina. Modelling of soil-structure interaction by finite and infinite elements. Technical Report 80/43, UCB/EERC, 1980.

[18] Ivar Stakgold. *Green's Functions and Boundary Value Problems*. Wiley-Interscience, 1979.

[19] Gilbert Strang and George J. Fix. *An Analysis of the Finite Element Method*. Automatic Computation. Prentice-Hall, 1973.

[20] John P. Wolf. *Dynamic Soil-Structure Interaction*. Prentice-Hall, 1985.

[21] John P. Wolf. The scaled boundary finite-element method – a fundamental solution-less boundary-element method. *Computer methods in applied mechanics and engineering*, 190:pp. 5551–5568, 2001.

[22] L. Ying. The infinite similar element method for calculating stress intensity factors. *Scientia Sinica*, 21:19–43, 1978.

[23] O. C. Zienkiewicz and R. L. Taylor. *The Finite Element Method*, volume 1. McGraw-Hill, New York, 4th edition, 1989.

A Appendix

A.1 Finite element stiffness matrix formulation

The stiffness matrix for the concave shape is constructed according to the conventional finite element formulation [23]. The small displacement strain is defined in terms of the chosen shape function:

$$\epsilon_{xx} = \sum_i^n u_i N_{i,x}(x,y), \quad \epsilon_{yy} = \sum_i^n v_i N_{i,x}(x,y), \quad \epsilon_{xy} = \sum_i^n \left(u_i N_{i,y}(x,y) + v_i N_{i,x}(x,y)\right).$$

In this first two dimensional example. The ground is considered to be infinitely thick and uniform. Accordingly the strain out of the plane should be zero while the stress may not be.

$$[C] = \frac{E}{(1+\nu)(1-2\nu)} \begin{bmatrix} 1-\nu & \nu & 0 \\ \nu & 1-\nu & 0 \\ 0 & 0 & \frac{1-2\nu}{2} \end{bmatrix}. \tag{24}$$

The stress is defined as a function of the strain.

$$\begin{Bmatrix} \sigma_x \\ \sigma_y \\ \sigma_{x,y} \end{Bmatrix} = [C].\begin{Bmatrix} \epsilon_x \\ \epsilon_y \\ \epsilon_{x,y} \end{Bmatrix} = [C].\begin{bmatrix} \{N_{i,x}(x,y)\} & \{0\} \\ \{0\} & \{N_{i,y}(x,y)\} \\ \{N_{i,y}(x,y)\} & \{N_{i,x}(x,y)\} \end{bmatrix}.\begin{Bmatrix} \{u_i\} \\ \{v_i\} \end{Bmatrix} \tag{25}$$

Define the stored strain energy functional $\frac{1}{2}\int_V \widetilde{\sigma}^T.\widetilde{\epsilon}\mathrm{d}V$ by substituting the matrix representations of the stress and strain:

$$\frac{1}{2}\int_V \langle \{u_i\} \quad \{v_i\} \rangle . \begin{bmatrix} \{N_{i,x}(x,y)\} & \{0\} & \{N_{i,y}(x,y)\} \\ \{0\} & \{N_{i,y}(x,y)\} & \{N_{i,x}(x,y)\} \end{bmatrix}.\begin{bmatrix} C_{11} & C_{12} & 0 \\ C_{12} & C_{22} & 0 \\ 0 & 0 & C_{33} \end{bmatrix}. \begin{bmatrix} \{N_{i,x}(x,y)\} & \{0\} \\ \{0\} & \{N_{i,y}(x,y)\} \\ \{N_{i,y}(x,y)\} & \{N_{i,x}(x,y)\} \end{bmatrix}.\begin{Bmatrix} \{u_i\} \\ \{v_i\} \end{Bmatrix} \mathrm{d}V. \tag{26}$$

The stiffness matrix is derived from the energy functional:

$$K_{ij}^{xx} = \int_V N_{i,x}(x,y) N_{j,x}(x,y)\mathrm{d}V, \quad K_{ij}^{xy} = \int_V N_{i,x}(x,y) N_{j,y}(x,y)\mathrm{d}V \tag{27}$$

and

$$K_{ij}^{yy} = \int_V N_{i,y}(x,y) N_{j,y}(x,y)\mathrm{d}V. \tag{28}$$

Substituting this into Eq. 26:

$$\frac{1}{2}\int_V \langle \{u_i\} \quad \{v_i\} \rangle . \begin{bmatrix} C_{11}[K^{xx}] + C_{33}[K^{yy}] & C_{12}[K^{xy}]^T + C_{33}[K^{xy}] \\ C_{12}[K^{xy}] + C_{33}[K^{xy}]^T & C_{22}[K^{yy}] + C_{33}[K^{xx}] \end{bmatrix} .. \begin{Bmatrix} \{u_i\} \\ \{v_i\} \end{Bmatrix} \mathrm{d}V \tag{29}$$

With respect to the plane strain example:

$$\begin{aligned}
[K_{\alpha\alpha}] &= \frac{E}{(1+\nu)(1-2\nu)}\left((1-\nu)[K^{xx}]+\frac{1}{2}(1-2\nu)[K^{yy}]\right)\\
[K_{\alpha\beta}] &= \frac{E}{(1+\nu)(1-2\nu)}\left(\frac{1}{2}(1-2\nu)[K^{xy}]^T+\nu[K^{xy}]\right)\\
[K_{\beta\beta}] &= \frac{E}{(1+\nu)(1-2\nu)}\left(\frac{1}{2}(1-2\nu)[K^{xx}]+(1-\nu)[K^{yy}]\right).
\end{aligned} \tag{30}$$

The element is then split into two parts: one pertaining to the displacement of the top boundary of the element and the other to the bottom boundary. The nodes on the top and the bottom boundary must be numbered in the same manner.

A.2 Conformal shape functions for convex and concave polygons

The following methods allow for the construction of Ritz coordinate functions which are smooth, linearly independent and bounded even within concave domains. Let the shape function for node (i) in a domain with (n) nodes be $N_i(x,y)$:

$$\begin{aligned}
N_i(x,y) &= \frac{s_i(x,y)}{\sum_i^n s_i(x,y)}\\
s_i(x,y) &= \prod_{i\neq j \ \&\ i\neq(j+1)}^{n} r_{j,(j+1)}(x,y)\\
r_{i,j}(x,y) &= l_i(x,y)-l_j(x,y)-l_{i,j}\\
l_i(x,y) &= \sqrt{(x_i-x)^2+(y_i-y)^2}\\
l_{i,j} &= l_i(x_j,y_j).
\end{aligned} \tag{31}$$

The resulting shape functions satisfy partition of unity and are bounded within the domain:

$$\sum_i^n N_i(x,y)=1 \quad \text{and} \quad 0<N_i(x,y)<1. \tag{32}$$

The details of the derivation, and variations on the shape function's form, are given in reference [16, 15]. For implementation details see [14].

In the given form, Equation 31, the shape functions do not satisfy linear fields:

$$\sum_i^n x_i N_i(x,y)\neq x \quad \text{and} \quad \sum_i^n y_i N_i(x,y)\neq y. \tag{33}$$

The limitation in the shape functions results in a stiffness matrix which produces energy when the element is rotated.

The derived shape functions $N_i(x,y)$ can be combined linearly so that they satisfy linear fields exactly:

$$\hat{N}_i(x,y)=N_{i-1}(x,y)w_{(i-1),i}(x,y)+N_i(x,y)w_{i,i}(x,y)+N_{i+1}(x,y)w_{i,(i+1)}(x,y). \tag{34}$$

Where $w_{i,j}$ is the normed barycentric coordinate for node (j) in the triangle defined by the verteces $(i-1, i, i+1)$. For example:

$$\hat{N}_3(x,y) = N_2(x,y)\frac{\triangle(\vec{x},1,2)}{\triangle(1,2,3)} + N_3(x,y)\frac{\triangle(\vec{x},4,2)}{\triangle(2,3,4)} + N_4(x,y)\frac{\triangle(\vec{x},4,5)}{\triangle(3,4,5)}. \tag{35}$$

The resulting functions $\hat{N}_i(x,y)$ satisfy the follwing:

$$\sum_i^n x_i\hat{N}_i(x,y) = x,\ \sum_i^n y_i\hat{N}_i(x,y) = y \quad \text{and} \quad \hat{N}_i(x,y) = 1. \tag{36}$$

The shape functions $\hat{N}_i(x,y)$ are linearly independent of one another but are not necessarily bounded in the domain. Both shape functions $N_i(x,y)$ and $\hat{N}_i(x,y)$ will be used in the cloning algorithm examples.